Self-interrupted synthesis of sterically hindered aliphatic polyamide dendrimers

Davit Jishkariani[a,1], Christopher M. MacDermaid[b,1], Yam N. Timsina[a,1], Silvia Grama[a], Syeda S. Gillani[a], Masoumeh Divar[a], Srujana S. Yadavalli[c], Ralph-Olivier Moussodia[a], Pawaret Leowanawat[a], Angely M. Berrios Camacho[a], Ricardo Walter[d,2], Mark Goulian[c], Michael L. Klein[b,3], and Virgil Percec[a,3]

[a]Roy and Diana Vagelos Laboratories, Department of Chemistry, University of Pennsylvania, Philadelphia, PA 19104-6323; [b]Institute of Computational Molecular Science, Temple University, Philadelphia, PA 19122; [c]Department of Biology, University of Pennsylvania, Philadelphia, PA 19104-6313 and [d]Department of Preventive and Restorative Sciences, School of Dental Medicine, University of Pennsylvania, Philadelphia, PA 19104-6030

Contributed by Michael L. Klein, February 7, 2017 (sent for review January 18, 2017; reviewed by Ezequiel Perez-Inestrosa and Donald A. Tomalia)

2,2-Bis(azidomethyl)propionic acid was prepared in four steps and 85% yield from the commercially available 2,2-bis(hydroxymethyl) propionic acid and used as the starting building block for the divergent, convergent, and double-stage convergent–divergent iterative methods for the synthesis of dendrimers and dendrons containing ethylenediamine (EDA), piperazine (PPZ), and methyl 2,2-bis(aminomethyl)propionate (COOMe) cores. These cores have the same multiplicity but different conformations. A diversity of synthetic methods were used for the synthesis of dendrimers and dendrons. Regardless of the method used, a self-interruption of the synthesis was observed at generation 4 for the dendrimer with an EDA core and at generation 5 for the one with a PPZ core, whereas for the COOMe core, self-interruption was observed at generation 6 dendron, which is equivalent to generation 5 dendrimer. Molecular modeling and molecular-dynamics simulations demonstrated that the observed self-interruption is determined by the backfolding of the azide groups at the periphery of the dendrimer. The latter conformation inhibits completely the heterogeneous hydrogenation of the azide groups catalyzed by 10% Pd/carbon as well as homogeneous hydrogenation by the Staudinger method. These self-terminated polyamide dendrimers are enzymatically and hydrolytically stable and also exhibit antimicrobial activity. Thus, these nanoscale constructs open avenues for biomedical applications.

dendrons | ethylenediamine core | piperazine core | antimicrobials | nanomedicine

Aliphatic polyamide (1–14) and peptide (15) dendrimers are complex monodisperse, functional compounds (16) synthesized by iterative divergent (1), convergent (17), and double-stage convergent–divergent (18) methods. Their nanoarchitecture emerges by increasing their generation number from ellipsoidal or disk-like 2D to 3D globular constructs (16, 19–25). Their core and branch multiplicities, as well as branch cell segment length (l), determine the generation number at which dendrimers become globular (19–21). Dendrimers synthesized by divergent iterative methods are expected to contain their functional groups, which increase in number with core and branch multiplicities as well as with their generation number, at the periphery of their 2D or 3D architectures (16, 19, 21). Dendrons and dendrimers produced by convergent strategies contain one functional group at their apex, whereas the rest of them are at their periphery (16, 17, 20, 23–25). Ultimately at a certain generation, dendrons also become globular dendrimers with their functional group from the apex becoming encapsulated at the core of the globular object (22–25). The large concentration of functional groups at the periphery of the globular object inspired a diversity of functions of biomedical interest that are not accessible with their linear homologs (26–31). Biomedical utility has propelled the field of aliphatic polyamide dendrimers to an unprecedentedly high level of expectations (26–31). Simultaneous with the interest in biomedical applications, it was predicted that a dense surface packing state generated by the presence of all functional groups on the periphery of the dendrimer would provide a critical packing state, above which a sterically inhibited reaction rate would be observed (32). Above this critical packing state, the lower reactivity of the functional groups on the periphery would provide globular dendrimers with incompletely reacted functional groups, thus generating an imperfect dendrimer structure (1, 2). Indeed, the most investigated, and best-elucidated, aliphatic polyamide [polyamidoamine (PAMAM)] dendrimer discovered and commercialized by Tomalia (Fig. 1) has been shown to exhibit an inhibited reaction rate of its functional groups at generations 4–7 as well as display a significant decrease in reaction rate at generations 7–8, although it could be synthesized with an imperfect structure up to generation 12 (2). Moreover, all other aliphatic polyamide dendrimers have been reported for only relatively low generations, without any explanation (Fig. 1).

This decrease in functional group reactivity on the surface of dendrimers was also explained by backfolding of peripheral groups (33, 34). Regardless of the mechanism that controls reactivity, the efficacy of a biomedical application is likely correlated with the reactivity of the peripheral functional groups of the dendrimer because incomplete interactions or reactions would generate, by analogy with iterative synthesis of higher dendrimer generations, an imperfect biologically active conjugated product. Herein, we report the divergent, convergent, and double-stage convergent–divergent iterative synthesis of a sterically hindered aliphatic polyamide dendrimer (12) by a diversity

Significance

Hydrolytically and enzymatically stable nanoscale synthetic constructs, with well-defined structures that exhibit antimicrobial activity, offer exciting possibilities for diverse applications in the emerging field of nanomedicine. Herein, we demonstrate that it is the core conformation, rather than periodicity, that ultimately controls the synthesis of sterically hindered aliphatic polyamide dendrimers. The latter self-interrupt at a predictable low generation number due to backfolding of their peripheral groups, which in turn leads to well-defined nanoarchitectures.

Author contributions: D.J., C.M.M., Y.N.T., S.S.Y., R.W., M.G., M.L.K., and V.P. designed research; D.J., C.M.M., Y.N.T., S.G., S.S.G., M.D., S.S.Y., R.-O.M., P.L., and A.M.B.C. performed research; D.J., C.M.M., Y.N.T., S.G., S.S.Y., R.-O.M., P.L., M.G., M.L.K., and V.P. contributed new reagents/analytic tools; D.J., C.M.M., Y.N.T., S.G., S.S.G., M.D., S.S.Y., R.-O.M., P.L., M.G., M.L.K., and V.P. analyzed data; and D.J., C.M.M., Y.N.T., S.G., S.S.Y., R.W., M.G., M.L.K., and V.P. wrote the paper.

Reviewers: E.P.-I., University of Malaga; and D.A.T., NanoSynthons LLC.

The authors declare no conflict of interest.

[1]D.J., C.M.M., and Y.N.T. contributed equally to this work.

[2]Present address: Department of Operative Dentistry, University of North Carolina, Chapel Hill, NC 27599-7450.

[3]To whom correspondence may be addressed. Email: percec@sas.upenn.edu or mlklein@temple.edu.

This article contains supporting information online at www.pnas.org/lookup/suppl/doi:10.1073/pnas.1700922114/-/DCSupplemental.

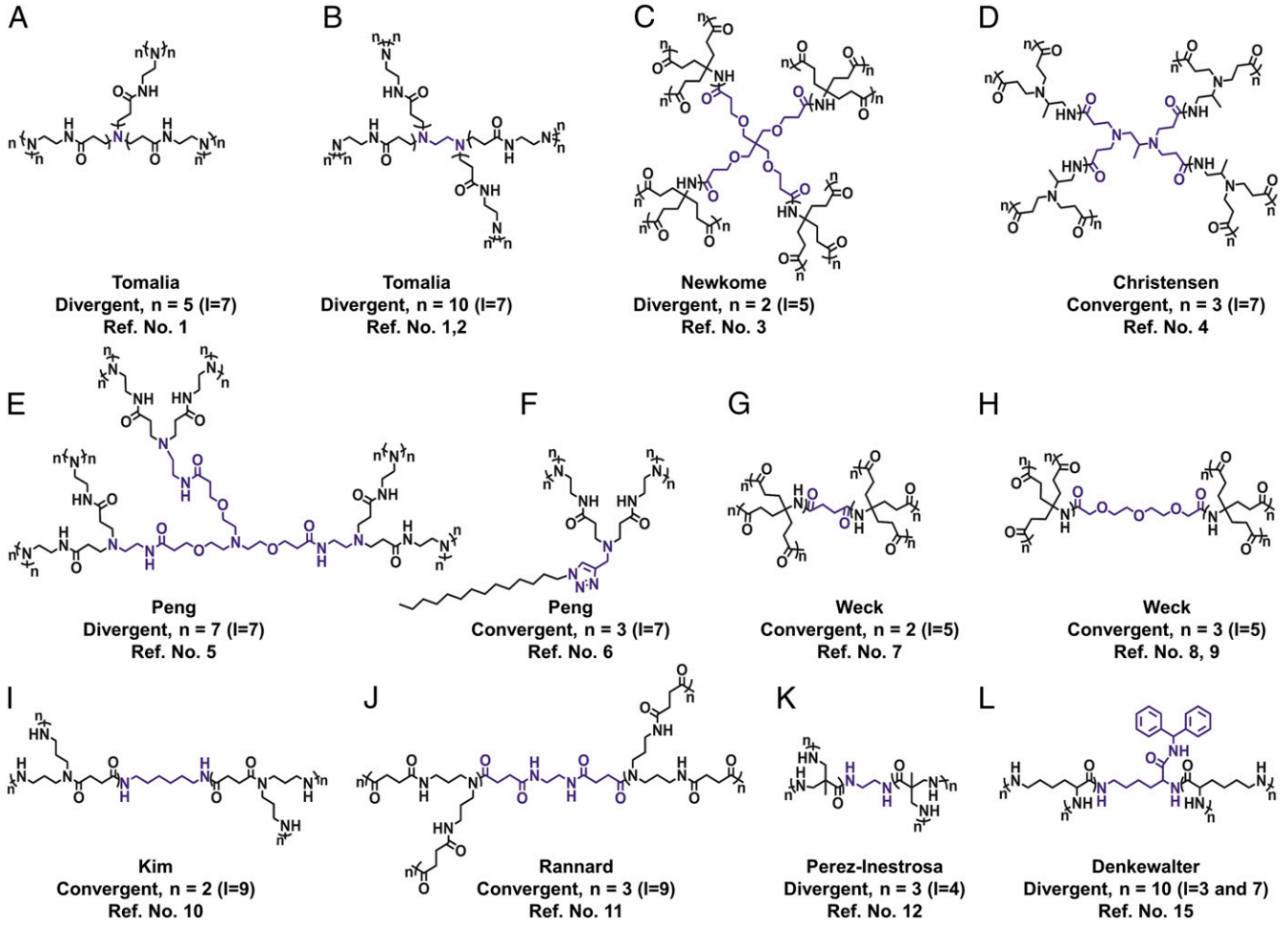

Fig. 1. (*A–L*) Name of the laboratory, synthetic method used, maximum generation number synthesized (n) of Gn, and the numbers of atoms in the linear part of their repeat unit or branch cell segment length (l, in-between parentheses) of aliphatic polyamide and peptide dendrimers reported in the literature.

of synthetic methods. Unexpectedly, self-interruption of the synthesis of this dendrimer was discovered at a generation that is determined by the conformation rather than the multiplicity of its core.

Results and Discussion

Selecting the Aliphatic Poly(amide) Dendrimer and the Synthesis of Its Building Block. The most sterically congested dendrimer reported to date (Fig. 1) (12) was selected to evaluate the reactivity of its functional groups as a function of generation number and core structure and compare it with nonsterically hindered aliphatic polyamide dendrimers.

This sterically hindered aliphatic polyamide dendrimer is expected to provide an amplification effect of the reactivity of similar functional groups available in less sterically hindered dendrimers. This sterically hindered aliphatic polyamide is also synthetically attractive because it was originally prepared from the inexpensive and commercially available 2,2-bis(hydroxymethyl)propionic acid AB_2 building block (**1** in Fig. 2) (12), which was previously used in the divergent iterative synthesis of five generations of aliphatic polyester dendrimers (35, 36) that are commercially available (37), as well as in the synthesis of amphiphilic Janus dendrimers that self-assemble in biomedically interesting dendrimersomes (38, 39).

The starting material for the iterative synthesis of the current aliphatic polyamide dendrimer is the AB_2 2,2-bis(azidomethyl)propionic acid (compound **7** in Fig. 2) that was previously obtained in 66% yield via the three reactions steps involving **1**, **2**, and **3** (Fig. 2) (12). Attempts to improve the low yield of this synthesis failed. Modification of this synthesis led to a more efficient four steps procedure involving **1**, **4**, **5**, and **6** to produce **7** in 85% yield while reducing the overall reaction time from 92 to 38 h (Fig. 2) and performing all steps under milder reaction conditions.

Divergent Synthesis of Four Dendrimer Generations with an Ethylenediamine Core. The first divergent synthesis investigated used a modified literature procedure that involved the use of an ethylenediamine (EDA) core and the acid chloride-activated form of **7** to produce three generations of polyamide dendrimers (12). The main modification involved the replacement of the amidation step consisting of the addition of **8** to a water/NaOH mixture containing EDA and a higher-generation dendrimer with the addition of **8** to a CH_2Cl_2/Et_3N solution of EDA at 0–23 °C (Fig. 2).

This modification improved the yield of the amidation step at all generations with a remarkable increase at G3 from 27 to 59%. We expect that, due to steric reasons, the rate of amidation of the acid chloride competes with its rate of hydrolysis, and therefore the transition from amidation in basic water to CH_2Cl_2 improved its yield (Fig. 2). The maximum generation of the previously reported synthesis of this dendrimer was G3 (12). Under the modified conditions used here, the maximum generation that could be synthesized with the EDA core was G4 (Fig. 2). All attempts to perform the heterogeneous reduction of the azide groups of G4 to amine with 10% Pd/C and up to stoichiometric amount of catalyst under 120 psi H_2 pressure as well as Staudinger homogeneous hydrogenation have failed. An amidation method inspired from the synthesis of peptides (40–42) was elaborated.

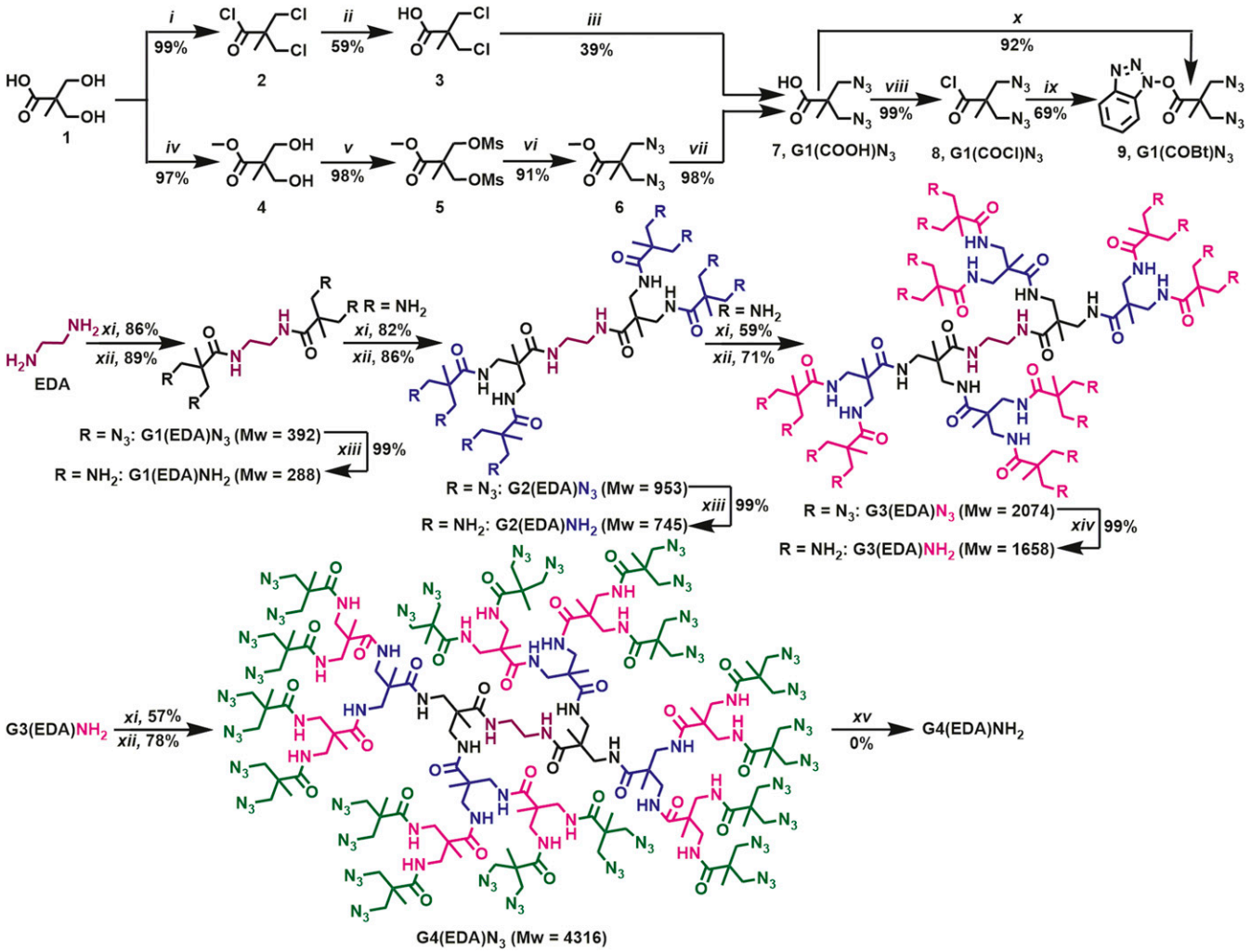

Fig. 2. Synthesis of 2,2-bis(azidomethyl)propionic acid, its carboxylic acid-activated forms, and the divergent synthesis of four generations of aliphatic polyamide dendrimers containing ethylenediamine (EDA) core. Reagents and conditions: (*i*) $SOCl_2$, dimethylformamide (DMF) (23 °C, 18 h, reflux, 24 h); (*ii*) H_2O, 7 M NaOH (0 °C, 2 h); (*iii*) NaN_3, DMF:H_2O (9:1) (80 °C, 48 h); (*iv*) MeOH, Amberlyst-15 (reflux, 5 h); (*v*) methanesulfonyl chloride (MsCl), triethylamine (Et_3N), CH_2Cl_2 (0–23 °C, 7 h); (*vi*) NaN_3, DMF (90 °C, 24 h); (*vii*) NaOH, MeOH/THF/H_2O [1/1/1 (vol/vol/vol)] (50 °C, 2 h); (*viii*) $SOCl_2$, CH_2Cl_2 (3 h, reflux); (*ix*) 1-hydroxybenzotriazole (HOBt), Et_3N, CH_2Cl_2 (0 °C, 0.5 h, then 23 °C, 12 h); (*x*) HOBt, *N,N′*-dicyclohexylcarbodiimide (DCC), 4-dimethylaminopyridine (DMAP), CH_2Cl_2 (23 °C, 1 h, then 35 °C, 2 h); (*xi*) **8**, Et_3N, CH_2Cl_2 (–78 °C, 0.5 h, then 23 °C, 12 h); (*xii*) **9**, Et_3N, CH_2Cl_2 (23 °C, 24 h); (*xiii*) 10% Pd/C [10% (wt/wt)], H_2 (120 psi) (23 °C, 2 h); (*xiv*) 10% Pd/C [30% (wt/wt)], H_2 (120 psi) (23 °C, 3 h); and (*xv*) 10% Pd/C [80% (wt/wt)], H_2 (120 psi) (23 °C, 3 h).

The carboxylic group of **7** was activated as an ester of 1-hydroxybenzotriazole (HOBt) either by the direct esterification of **7** with HOBt in the presence of *N,N′*-dicyclohexylcarbodiimide (DCC) and a catalytic amount of 4-dimethylaminopyridine (DMAP) to produce **9** in 92% yield or by the esterification of **8** in the presence of Et_3N to generate **9** in only 69% yield. Amidation of EDA followed by iterative reduction/amidation steps produced consistently four generations of dendrimers in up to 20% higher yields than the acid chloride methods (Fig. 2). However, the reduction of G4(EDA)N_3 generated by the HOBt-activated method could not be accomplished.

Divergent Synthesis of Five Dendrimer Generations with a Piperazine Core. Disubstituted EDA and piperazine (PPZ) exhibit the same multiplicity but different conformations (43–45). The same core multiplicity with different conformations was not previously investigated in the synthesis of dendrimers (1, 2, 16, 46). The divergent iterative methods based on the acid chloride **8** and the HOBt ester **9** of **7** were both used in the synthesis of polyamide dendrimers. High yields (63–92%) were obtained for the first four generations with both methods (Fig. 3). However, by contrast with the EDA core that allowed the synthesis of only four generations, the PPZ generated five generations of dendrimers. G5(PPZ)N_3 was obtained in 44–38% yield with both methods. Attempts to hydrogenate G5(PPZ)N_3 to G5(PPZ)NH_2 failed.

Divergent Synthesis of Six Dendron Generations. The focal point of the polyamide dendrons was generated by the reduction of the azide groups of G1(COOMe)N_3 (compound **6** from Fig. 2) to NH_2 to generate G1(COOMe)NH_2 in 98% yield (Fig. 4). Amidation of G1(COOMe)NH_2 with **9** (Fig. 2) or with **8** (Fig. 2) produced G2(COOMe)N_3 in 92% and 84% yield, respectively (Fig. 4). Hydrolysis of the methyl ester of G2(COOMe)N_3 produced G2(COOH)N_3 in 93% yield (Fig. 4). Activation of the COOH group of G2(COOH)N_3 as HOBt ester or as acid chloride followed by amidation with G1(COOMe)N_3 produced G3(COOMe)N_3 (85% and 55% yields), which was hydrolyzed to G3(COOH)N_3 (91% yield) (Fig. 4).

Reduction of the azide groups of G2(COOMe)N_3 to G2(COOMe)NH_2 (94% yield) followed by its amidation with **9** produced G3(COOMe)N_3 (60% yield), which was reduced to G3(COOMe)NH_2 (95% yield) and amidated with **9** to generate

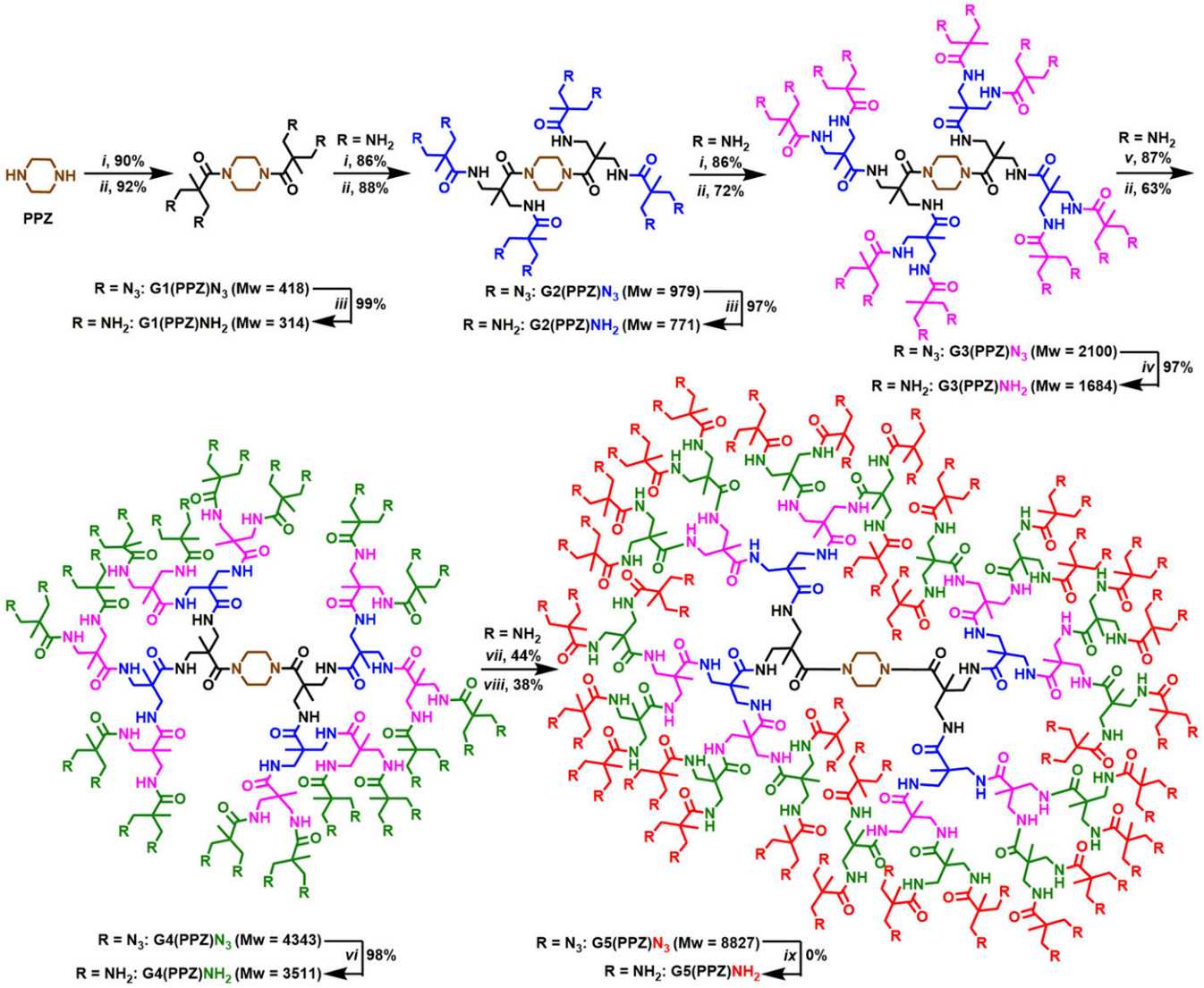

Fig. 3. Divergent synthesis of five generations of aliphatic polyamide dendrimers containing piperazine (PPZ) core. Reagents and conditions: (*i*) **9**, Et_3N, CH_2Cl_2 (23 °C, 24 h); (*ii*) **8**, Et_3N, CH_2Cl_2 (–78 °C, 0.5 h, then 23 °C, 12 h); (*iii*) 10% Pd/C [15% (wt/wt)], H_2 (120 psi) (23 °C, 3 h); (*iv*) 10% Pd/C [20% (wt/wt)], H_2 (120 psi) (23 °C, 3 h); (*v*) **9**, Et_3N, CH_2Cl_2 (23 °C, 48 h); (*vi*) 10% Pd/C [50% (wt/wt)], H_2 (120 psi) (23 °C, 8 h); (*vii*) **9**, Et_3N, CH_2Cl_2 (23 °C, 72 h); (*viii*) **8**, Et_3N, CH_2Cl_2 (–78 °C, 1 h, then 23 °C, 24 h); and (*ix*) 10% Pd/C [80% (wt/wt)], H_2 (120 psi) (23 °C, 8 h).

$G4(COOMe)N_3$ (49% yield) that was reduced to $G4(COOMe)NH_2$ in 92% yield. Repeating this amidation/reduction iteration on $G4(COOMe)NH_2$ produced $G5(COOMe)NH_2$ in 40% yield. Amidation of G5 with **9** produced $G6(COOMe)N_3$ in 38% yield. All attempts to reduce the azide groups of $G6(COOMe)N_3$ to $G6(COOMe)NH_2$ failed. This is not surprising because the $G6(COOMe)N_3$ dendron is equivalent to a G5 dendrimer that contains at the focal point the methyl ester of 2,2-bis(aminomethyl) propionic acid (Fig. 4).

This focal point has the same multiplicity as EDA (Fig. 2) and PPZ (Fig. 3) except that it contains an additional tetrahedral carbon isolating the methylenic units from EDA or PPZ (Fig. 4).

Accelerated Double-Stage Convergent–Divergent Synthesis of Three EDA Generations and Five PPZ Generations of Dendrimers. An accelerated double-stage convergent-divergent synthesis was also used for the synthesis of dendrimers containing EDA and PPZ at their core (Fig. 5). $G2(COOH)N_3$ (Fig. 4) was activated both as HOBt ester and as acid chloride (both in 99% conversion and used without purification) (Fig. 5), whereas $G3(COOH)N_3$ (Fig. 4) was activated only as HOBt ester (99% conversion and used without purification). These activated compounds were reacted with EDA and PPZ to produce $G2(EDA)N_3$ (78% yield), $G2(PPZ)N_3$ (65% yield), $G3(EDA)N_3$ (78% yield), and $G3(PPZ)N_3$ (65% yield) (Fig. 5). Amidation of $G2(PPZ)NH_2$ (Fig. 3) with $G2(COBt)N_3$ and $G2(COCl)N_3$ generated $G4(PPZ)N_3$ in 16% and 42% yields (Fig. 5).

Finally, $G3(COBt)N_3$ was reacted with $G2(PPZ)NH_2$ to produce $G5(PPZ)N_3$ in 18% yield. Repeated attempts to reduce the azide groups of $G5(PPZ)N_3$ to generate $G5(PPZ)NH_2$ did not succeed.

Structural Analysis of Dendrimers and Dendrons. Structural analysis of all dendrimers and dendrons prepared by divergent and accelerated double-stage convergent–divergent methods by a combination of 500-MHz ^{1}H-NMR (*SI Appendix*, Figs. S1 and S2), 126-MHz ^{13}C-NMR spectroscopy (*SI Appendix*, Figs. S3 and S4), gel permeation chromatography (GPC) (Fig. 6*A*), and matrix-assisted laser desorption/ionization time of flight (MALDI-TOF) (Fig. 6*B*) demonstrated perfectly monodisperse compounds with molar masses equal to their theoretical values. This demonstrates that, although the reactivity of the azide and amine groups from their periphery may decrease while the generation

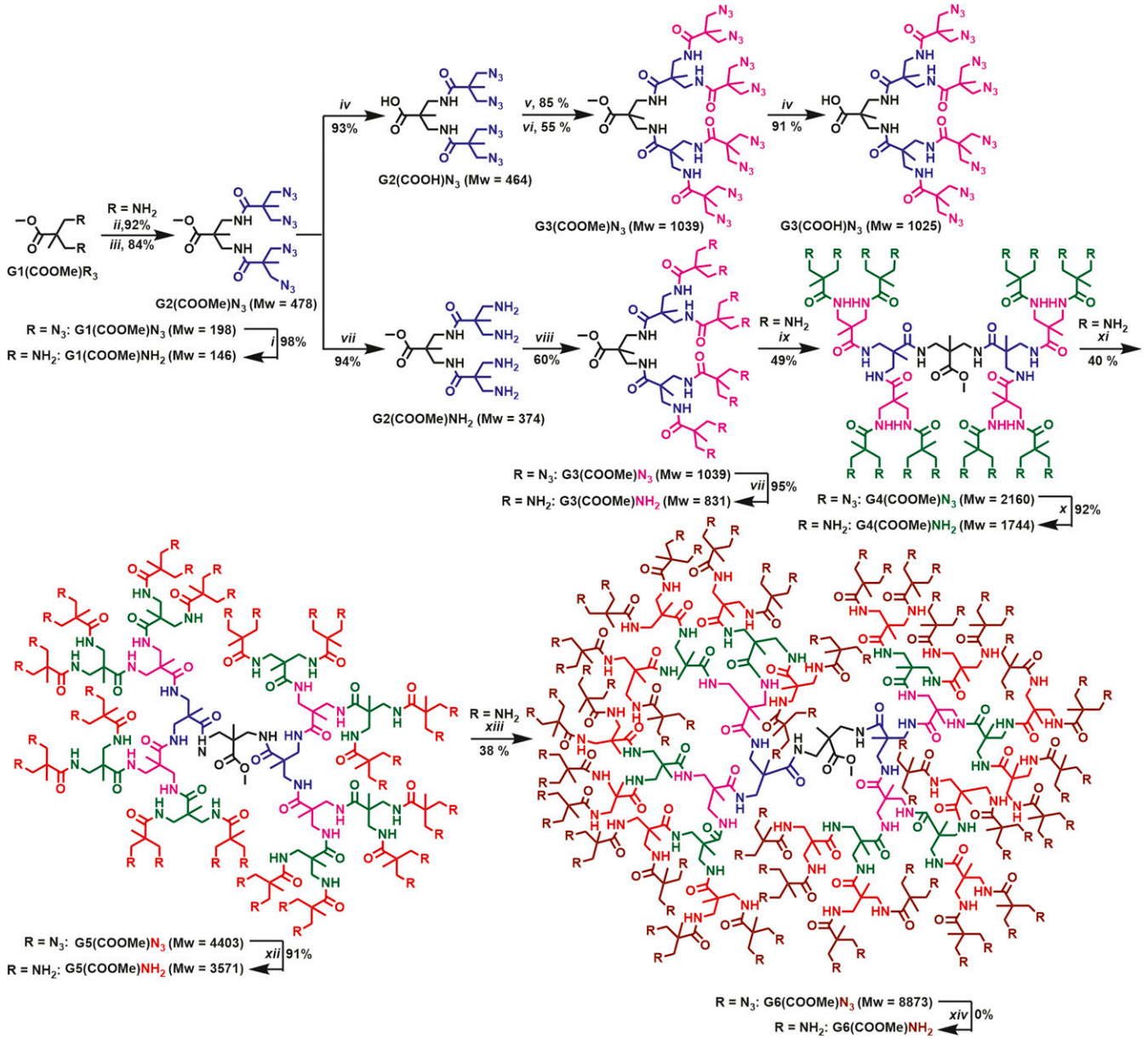

Fig. 4. Synthesis of the methyl ester of 2,2-bis(aminomethyl)propionic acid, the convergent synthesis of three generations, and the divergent synthesis of six generations of aliphatic polyamide dendrons. Reagents and conditions: (*i*) 10% Pd/C [10% (wt/wt)], H_2 (120 psi), MeOH (23 °C, 3 h); (*ii*) **9**, Et_3N, CH_2Cl_2 (23 °C, 24 h); (*iii*) **8**, Et_3N, CH_2Cl_2 (–78 °C, 0.5 h, then 23 °C, 12 h); (*iv*) NaOH, THF/MeOH/H_2O [1/1/1 (vol/vol/vol)] (50 °C, 2 h); (*v*) DCC, HOBt, CH_2Cl_2 (23 °C, 6 h, then 35 °C, 2 h), then G1(COOMe)NH_2, Et_3N, CH_2Cl_2, (23 °C, 24 h); (*vi*) $SOCl_2$, CH_2Cl_2 (reflux, 4 h), then G1(COOMe)NH_2, Et_3N, CH_2Cl_2 (–78 °C, 0.5 h, then 23 °C, 15 h); (*vii*) 10% Pd/C [10% (wt/wt)], H_2 (120 psi), MeOH (23 °C, 2 h); (*viii*) **9**, Et_3N, CH_2Cl_2 (23 °C, 24 h); (*ix*) **9**, Et_3N, CH_2Cl_2 (23 °C, 48 h); (*x*) 10% Pd/C [20% (wt/wt)], H_2 (120 psi), MeOH (23 °C, 2 h); (*xi*) **9**, Et_3N, CH_2Cl_2 (23 °C, 48 h); (*xii*) 10% Pd/C [30% (wt/wt)], H_2 (120 psi), MeOH (23 °C, 2 h); (*xiii*) **9**, Et_3N, CH_2Cl_2 (23 °C, 48 h); and (*xiv*) 10% Pd/C [80% (wt/wt)], H_2 (120 psi), MeOH (23 °C, 2 h).

number increases, there is a generation number at which at least the azide groups become completely inactive toward heterogeneous hydrogenation catalyzed with 10% Pd/C as well as homogeneous hydrogenation by the Staudinger reaction. This lack of reactivity produces a self-interruption of the dendrimer synthesis process. Notably, this generation number is controlled by the structure of the core even when the multiplicity of the core is identical. This demonstrates that the conformation of the core is either as important or even more important than its multiplicity.

Molecular Modeling and Molecular-Dynamics Simulations of Azido-Terminated Dendrimers. Long-timescale fully atomistic molecular-dynamics simulations, based on state-of-the-art force fields, demonstrate that the observed decrease in reactivity of the dendrimer's peripheral groups is commensurate with increasing sequestration of these groups and an overall compactness of the dendrimer. Calculated atom number densities and radial distribution functions (Figs. 7 and 8) indicate that an increasing number of terminal groups are backfolded into the dendrimer interior or are trapped in invaginations created on the dendrimers surface.

The calculated radius of gyration of the peripheral groups $R_g(N_3)$, demarcated by the solid white line in the density contours of Fig. 7, is only slightly greater than the radius of gyration of the dendrimer (inner gray line), but always much less than that of its calculated radius of solvent accessible surface area (r_{SASA}, outer gray line), indicating a tightly compact structure.

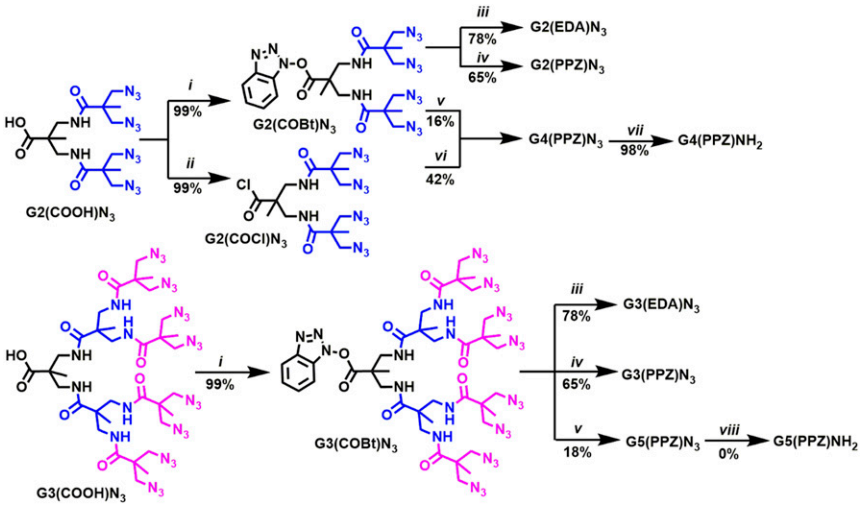

Fig. 5. Accelerated double-stage convergent–divergent synthesis of three EDA generations and five PPZ generations of aliphatic polyamide dendrimers. (*i*) HOBt, DCC, CH_2Cl_2 (23 °C, 1 h, then 35 °C, 5 h); (*ii*) $SOCl_2$, CH_2Cl_2 (reflux, 4 h); (*iii*) EDA, Et_3N, CH_2Cl_2 (23 °C, 24 h); (*iv*) PPZ, Et_3N, CH_2Cl_2 (23 °C, 24 h); (*v*) G2(PPZ)NH_2, Et_3N, CH_2Cl_2 (23 °C, 12 h); (*vi*) G2(PPZ)NH_2, Et_3N, CH_2Cl_2 (–78 °C, 0.5 h, then 23 °C, 12 h); (*vii*) 10% Pd/C [50% (wt/wt)], H_2 (120 psi) (23 °C, 8 h); (*viii*) 10% Pd/C [80% (wt/wt)], H_2 (120 psi) (23 °C, 8 h).

This ratio, $R_g(N_3)/r_{SASA}$ is always less than 1 and decreases as the dendrimer generation increases, indicating a propensity of the outer groups to compact into the dendrimer structure, rather than expand into the bulk solvent. This presumably leads to the observed decrease and eventual cessation of their reactivity. Furthermore, and most importantly, this ratio is also dependent on the chosen core type, with the $R_g(N_3)/r_{SASA}$ decrease per generation being most pronounced for the EDA core, followed by that of PPZ and finally COOMe. Thus, the computations fully support the observation that the chosen core type influences the reactivity of the peripheral groups, with the most rigid core having the most pronounced effect. Last, the calculated radial distribution functions, $\rho(r)$ show a nonzero probability of finding terminal groups (Fig. 8, solid teal line) backfolded into the dendrimer. Calculated 3D atom number densities (Fig. 7, yellow hotspots) indicate buried terminal groups as well.

Given the observed compactness of the dendrimer's structure, we wondered whether reactants could penetrate into the dendritic interior to react with the buried terminal groups. Using a spherical probe with various radii, the surface areas of the model dendrimers were calculated. Because the square root of the surface area of a sphere is linearly proportional to the probe radius, any computed deviations from linearity between these values indicate penetration by the probe into the dendrimer interior. Only a smaller probe can penetrate into surface invaginations, leading to an apparent increase in surface area. Deviations are indeed observed with probe radii less than ~3 Å (Fig. 9) beginning with the fourth-generation dendrimer and are more pronounced at smaller probe radii and larger dendrimer generations.

This suggests that, in order for reactants to penetrate the surface of the dendrimer, they must have an apparent radius less than ~3 Å, or about the average distance between two oxygen atoms in bulk water. Couple this with the likelihood for the reactant molecule to at least partially desolvate to penetrate, and the observed decrease in reactivity of the terminal groups becomes quite clear.

Antimicrobial Properties of Dendrimers and Susceptibility to Enzymatic and Chemical Hydrolysis. Naturally occurring peptides as well as synthetic mimics including peptoids are known to exhibit antimicrobial activities (47–53). To test for potential antimicrobial activity of the present aliphatic polyamide dendrimers terminated with amine, cell viability assays using resazurin were performed.

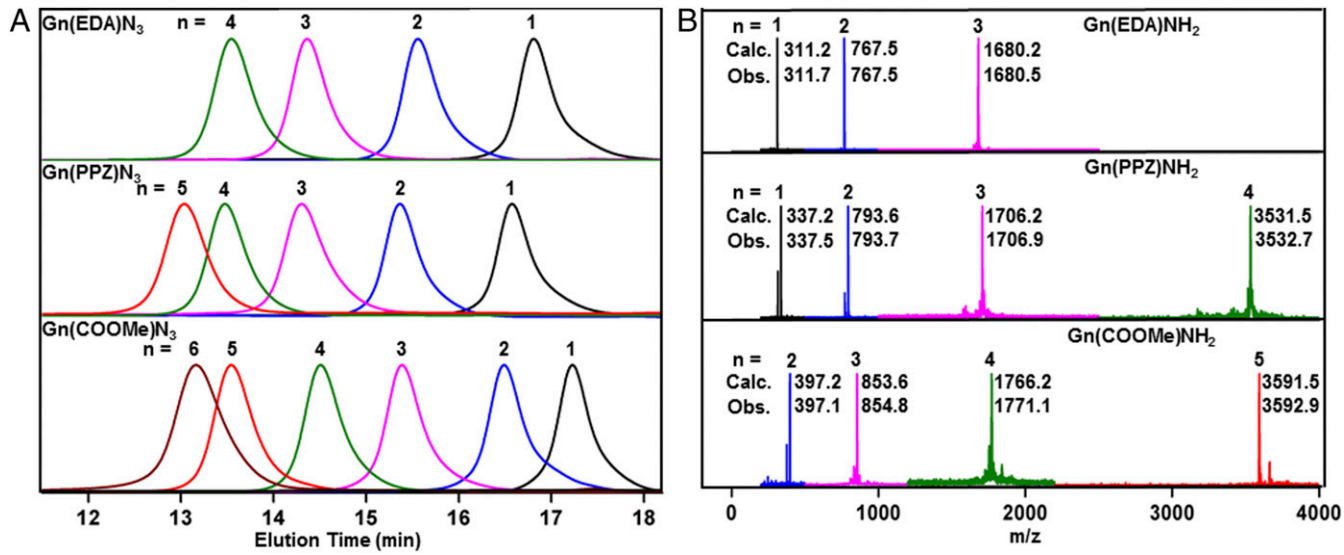

Fig. 6. GPC traces (*A*) of Gn(EDA)N_3 (n = 1–4) and Gn(PPZ)N_3 (n = 1–5) dendrimers and Gn(COOMe)N_3 (n = 1–6) dendrons and MALDI-TOF spectra (*B*) of Gn(EDA)NH_2 (n = 1–3) and Gn(PPZ)NH_2 (n = 1–4) dendrimers and Gn(COOMe)NH_2 (n = 2–5) dendrons. Calc. and Obs. are the molecular weights calculated and observed in the presence of sodium ions $[M+Na]^+$.

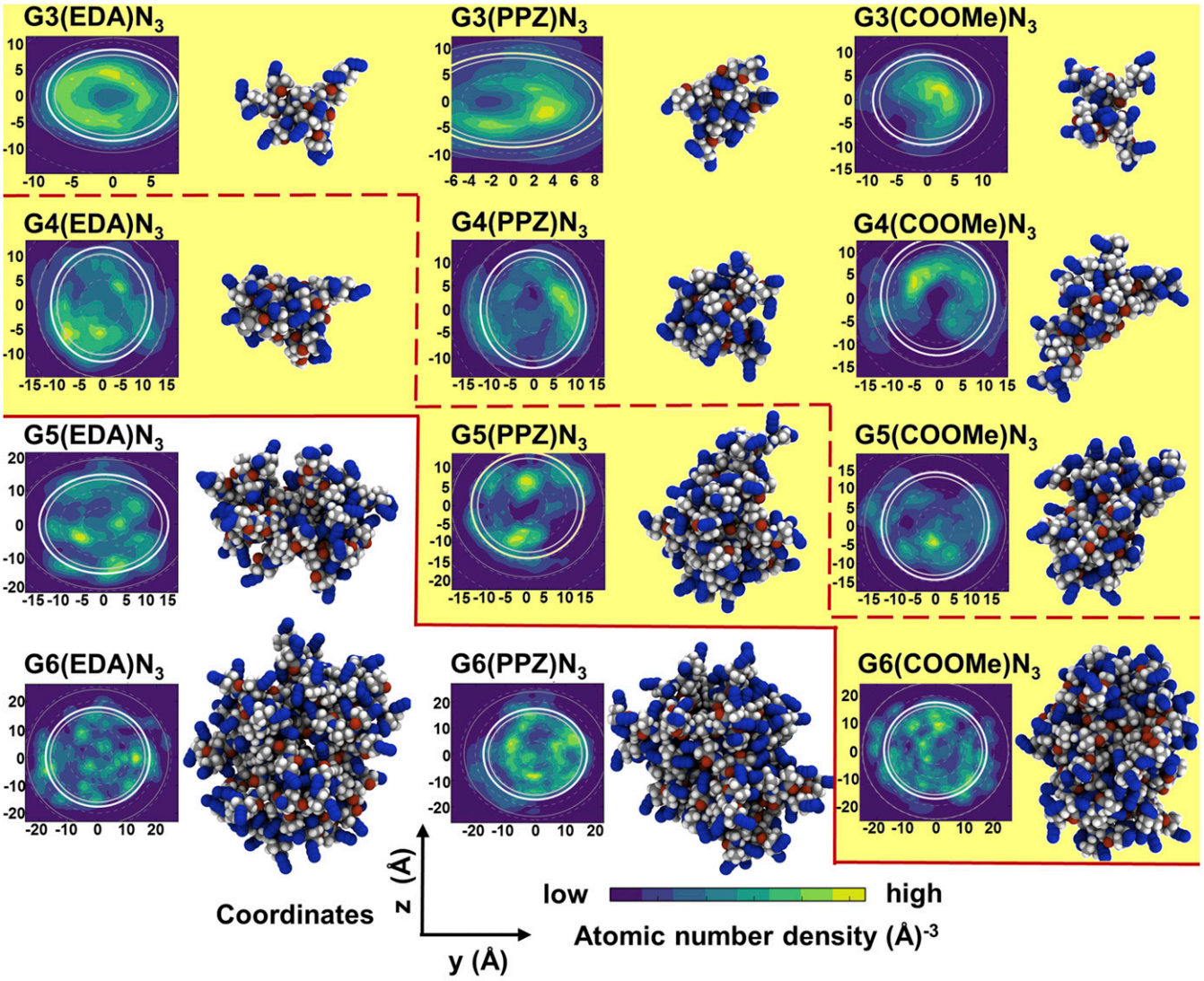

Fig. 7. Two-dimensional slices of the 3D average atom number densities (in atoms per cubic angstrom) of the terminal N_3 groups, and molecular renders for Gn(EDA)N_3 (n = 3–6), Gn(PPZ)N_3 (n = 3–6) dendrimers, and Gn(COOMe)N_3 (n = 3–6) dendrons. Continuous red line marks the maximum generation number synthesized for the azide dendrimers with EDA, PPZ, and COOMe cores. Dotted red line marks the maximum generation number of the azide dendrimers that could be hydrogenated to the corresponding amines. In the molecular renders, carbon atoms are colored gray; nitrogen, blue; oxygen, red; and hydrogen, white. The number density contours are centered on the dendrimer's center of mass ($x = 0$, $z = 0$) and look along the x axis. Dashed gray lines demarcate radial separations of 5 Å. The solid lines denote calculated properties: the radius of gyration (R_g) of the dendrimer (inner gray line), the R_g of the terminal N_3 groups (thick white line), and the radius of the solvent-accessible surface area (r_{SASA}) (outer gray line).

Resazurin is a redox indicator dye, which provides a readout for bacterial cell growth and viability (54). The minimal inhibitory concentration (MIC) is measured as described in *Methods*. G4(PPZ)NH_2 was found to be active against all Gram-positive bacteria that were tested (*Bacillus subtilis*, *Bacillus cereus*, *Micrococcus luteus*, and *Staphylococcus aureus*—see *SI Appendix*, Table S2, for MIC estimates). G2(PPZ)NH_2 did not display antibacterial activity at concentrations up to 1,024 μg/mL.

To test susceptibility to enzymatic hydrolysis, polyamide dendrimers G2(PPZ)NH_2, G4(PPZ)NH_2, and G4(PPZ)N_3 were treated with a broad-spectrum protease, proteinase K (EC 3.4.21.64) (55), which is a serine protease with a broad specificity toward peptide substrates, and analyzed by ^{1}H NMR and MALDI-TOF (*Methods*). All three dendrimers were found to be stable against enzymatic degradation (*Methods* and *SI Appendix*). The hydrolytic stability of these dendrimers was tested for 24 h at 23 °C and 80 °C under base-catalyzed conditions for G4(PPZ)N_3 and for G3(EDA)NH_2 under acid-catalyzed conditions. Unexpectedly, no hydrolysis was observed under any of these conditions (*Methods* and *SI Appendix*). The enzymatic and hydrolytic stability of these aliphatic polyamide dendrimers make them likely candidates for biomedical applications.

Conclusions

Sterically hindered aliphatic polyamide dendrimers are expected to amplify the dependence of the reactivity of their peripheral functional groups on their core structure and generation number. Understanding this reactivity–core structure–generation dependence is important to elucidate the synthesis of such constructs for potential applications in nanomedicine. Toward this goal, a study of the divergent, convergent, and double-stage convergent–divergent iterative synthesis of the most sterically hindered polyamide dendrimer known to date (12) was performed in gram quantities (Fig. 10) with three different cores (EDA, PPZ, COOMe) having the same multiplicity but different conformations.

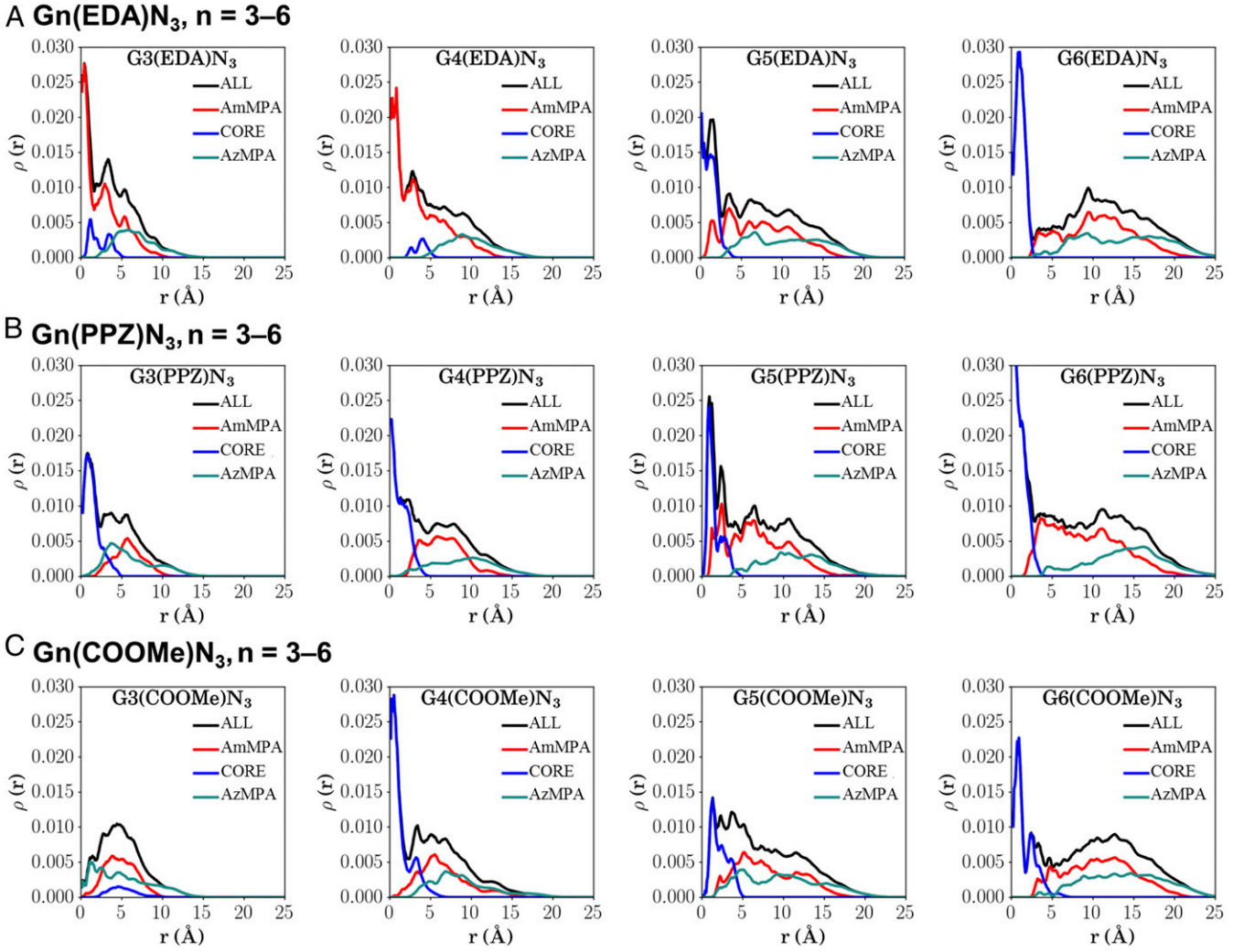

Fig. 8. Radial distribution functions $\rho(r)$ of (*A*) Gn(EDA)N_3 (n = 3–6), (*B*) Gn(PPZ)N_3 (n = 3–6) dendrimers, and (*C*) Gn(COOMe)N_3 (n = 3–6) dendrons. The calculations were done using the dendrimer and dendron center of mass as a reference (r = 0 Å). The unit value for $\rho(r)$ is expressed in atoms per cubic angstrom and quantifies the number of atoms in the volume element given by $4\pi r^2$. The abbreviations in the legends stand for the following: ALL, Gn(EDA/PPZ/COOMe)N_3 dendrimer or dendron; AmMPA, 2,2-bis(aminomethyl)propionic acid repetitive units; AzMPA, 2,2-bis(azidomethyl)propionic acid unit; CORE, EDA/ PPZ/COOMe. Note that, regardless of core type, there exists a nonzero terminal group density within the dendrimer (teal line) indicating backfolding and sequestering of the terminal azido groups away from the dendrimer surface.

A four-step synthesis in high yield, short reaction time, and under mild reaction conditions of the starting compound [2,2-bis(azidomethyl)propionic acid obtained from the commercial 2,2-bis(hydroxymethyl)propionic acid] was elaborated to facilitate this study. Unexpectedly, the conformation rather than the multiplicity of the core provided self-interruption of the iterative synthesis at a predictable generation number. These results expand on previous work that predicted and demonstrated a change in the reactivity of the functional groups for less sterically hindered polyamide dendrimers such as PAMAM (1, 2, 32). Molecular modeling and molecular-dynamics simulations demonstrated that this self-interruption is likely due to the backfolding of the functional groups on the dendrimer periphery. The steric hindrance of these aliphatic polyamide dendrimers makes them behave like peptoids (53) rather than as peptides of β-amino acids, and consequently they are both enzymatically and hydrolytically stable. While demonstrating self-interruption synthesis of sterically hindered aliphatic polyamide dendrimers, these experiments also provided quantitative mechanistic insights into the De Gennes self-limiting growth and dense packing parameters (32). This combination of function together with their gram quantity synthesis, and their antimicrobial properties, make these dendrimer nanoarchitectures interesting candidates for nanomedicine.

Methods

Synthesis of Dendrimers and Dendrons. Dendrimers and dendrons were synthesized by divergent, convergent, and double-stage convergent–divergent iterative methods starting from the commercially available 2,2-bis(hydroxymethyl)propionic acid. Details of their synthesis and structural analysis methods and data are available in *SI Appendix*.

In Silico Modeling and Molecular-Dynamics Simulations. The monomers used in constructing models of the dendrimer macromolecules were taken from ref. 12. The molecules were described by the Amber GAFF forcefield (56) except for the terminal azido group for which parameters were used from previous work (57). Fully atomistic molecular-dynamics simulations were performed using NAMD 2.11 (58). The NPT ensemble was applied with a temperature of 300 K and a pressure of 1.0 atm. Methanol was used as a solvent and was described using the Amber force field. A time step of 1 fs was used. Trajectories of each of the 18 systems (3 cores, 6 generations each) were collected for a minimum of 100 ns, of which the last 20 ns was used for analysis. Dendrimer rmsd and autocorrelation functions of the square of the radius of gyration were used to establish equilibrium and relevant decorrelation

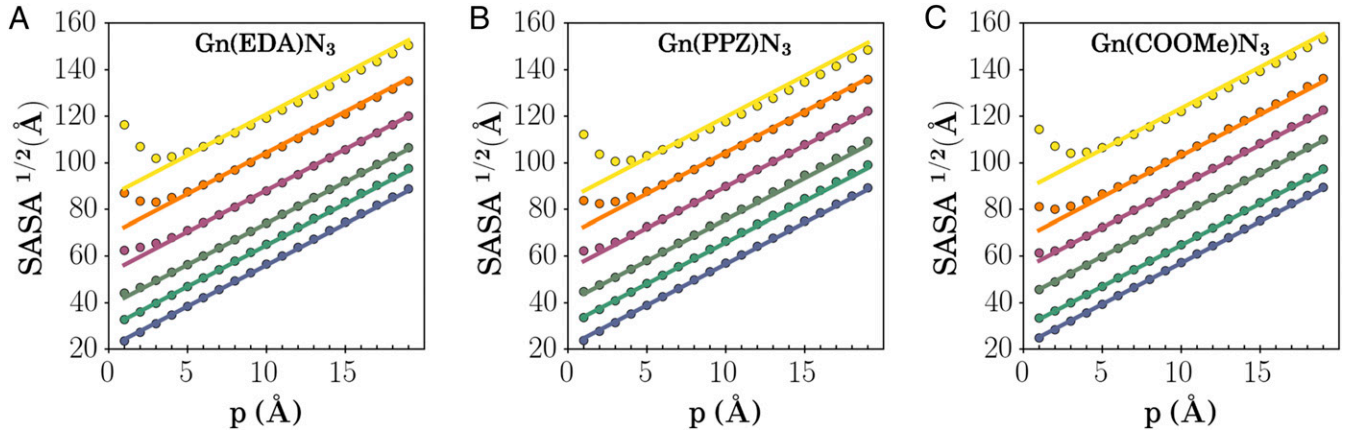

Fig. 9. Square root of solvent-accessible surface area (SASA) as a function of probe radius p for (*A*) Gn(EDA)N_3 (n = 1–6) and (*B*) Gn(PPZ)N_3 (n = 1–6) dendrimers, and (*C*) Gn(COOMe)N_3 (n = 1–6) dendrons. Color code: blue (n = 1), green (n = 2), gray (n = 3), red (n = 4), orange (n = 5), and yellow (n = 6). Deviations from linearity indicate probe sizes necessary to penetrate the dendrimer surface and explore small cavities and surface invaginations. For generations n = 4–6, probe sizes less than $r \sim 3$ Å are required for penetration, suggesting that reactants must be at least this small to interact with the sequestered 2,2-bis(azidomethyl)propionic acid (AzMPA) groups.

times. The VMD software package (59) was used to perform the following analyses: the radial distribution function, autocorrelation function, radius of gyration, solvent-accessible surface area, fractal dimension, and aspect ratios. The MD analysis package (60) was used to calculate the 3D atomic densities. Thorough accounts of the modeling and simulation details are available in *SI Appendix*.

Cell Viability Assays Using Resazurin. Cell viability assays to determine MICs were performed using resazurin based on established protocols (61). Saturated cultures of the strains to be tested were grown in Mueller Hinton broth (MHB) (Difco) at 37 °C with aeration for 16–18 h. The cultures were then diluted 1:100 in fresh MHB and allowed to grow to an optical density at 600 nm (OD_{600}) of ∼0.2. A 2× dilution scheme of the test dendrimer was prepared in MHB in a 96-well clear microtiter plate such that the final concentrations were 0, 1, 2, 4, 8, 16, 32, 64, 128, 256, 512, and 1,024 μg·mL^{-1} in a 50-μL volume. Five microliters of 0.675% resazurin stock solution was added to each well containing the dendrimer solution. Cultures grown to OD_{600} were diluted 1:100 fold and 50 μL of cells were added to each well. The plate was placed on a shaker for 15 min, followed by stationary incubation at 37 °C for 16–18 h. For *M. luteus*, the incubation was carried out for ∼48 h as the strain grows slowly at 37 °C. Resazurin turns from blue to pink color as a function of cell growth. A MIC value was determined by the lowest concentration of dendrimer at which there was no color change. All estimates were derived from at least three independent trials.

Proteinase K Digestion. Proteinase K digestions of the dendrimers terminated with an amine group were performed as follows: 5 mg of the dendrimer G2(PPZ)NH_2 or G4(PPZ)NH_2 was added to 5 mg of proteinase K in a microcentrifuge tube and resuspended in 200 μL of 30 mM Tris·HCl, pH 8. A control for proteinase K without addition of dendrimer was included. The tubes were incubated at 37 °C overnight. Following ∼16 h at 37 °C, the above reactions were dehydrated at room temperature in a Speedvac to facilitate analysis of samples by NMR and MALDI-TOF. All of the

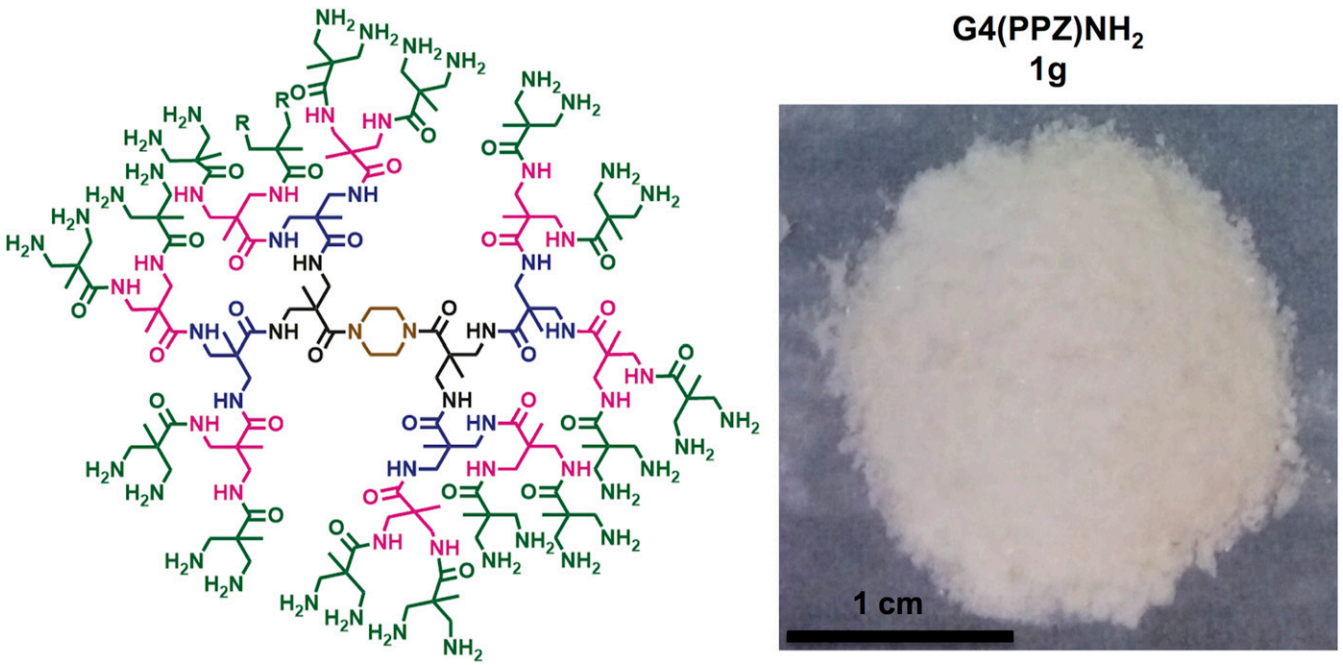

Fig. 10. Gram-scale synthesis of G4(PPZ)NH_2 using the 1*H*-benzo[*d*][1,2,3]triazol-1-yl-2,2-bis(azidomethyl)propanoate, **9**.

dendrimers were recovered, and their structures were confirmed by NMR and MALDI-TOF.

ACKNOWLEDGMENTS. This work was supported by National Science Foundation Grants DMR-1066116 and DMR-1120901 (to V.P.), the P. Roy Vagelos Chair at the University of Pennsylvania (to V.P.), the Humboldt Foundation (V.P.), the Joseph and Josephine Rabinowitz Award for Excellence in Research from the School of Dental Medicine at the University of Pennsylvania (to V.P. and R.W.), National Science Foundation Grant DMR-1120901 (to M.L.K. and M.G.), and National Institutes of Health Grant R01-GM080279 (to M.G.). Computer time was provided through National Science Foundation Grant ACI-1614804, the Petascale Computing Resource Allocations allocation baeg, and generous support from the National Center for Supercomputer Applications (C.M.M. and M.L.K.).

1. Tomalia DA, et al. (1985) A new class of polymers: Starburst-dendritic macromolecules. *Polym J* 17(1):117–132.
2. Tomalia DA, Naylor AM, Goddard WA (1990) Starburst dendrimers: Molecular-level control of size, shape, surface chemistry, topology and flexibility from atoms to macroscopic matter. *Angew Chem Int Ed Engl* 29(2):138–175.
3. Newkome GR, Yao Z, Baker GR, Gupta VK (1985) Cascade molecules: A new approach to micelles. A [27]-Arborol. *J Org Chem* 50(11):2003–2004.
4. Pittelkow M, Christensen JB (2005) Convergent synthesis of internally branched PAMAM dendrimers. *Org Lett* 7(7):1295–1298.
5. Liu XX, et al. (2009) PAMAM dendrimers mediate siRNA delivery to target Hsp27 and produce potent antiproliferative effects on prostate cancer cells. *ChemMedChem* 4(8): 1302–1310.
6. Liu X, et al. (2011) Structurally flexible triethanolamine core PAMAM dendrimers are effective nanovectors for DNA transfection in vitro and in vivo to the mouse thymus. *Bioconjug Chem* 22(12):2461–2473.
7. Yoon K, Goyal P, Weck M (2007) Monofunctionalization of dendrimers with use of microwave-assisted 1,3-dipolar cycloadditions. *Org Lett* 9(11):2051–2054.
8. Ornelas C, Broichhagen J, Weck M (2010) Strain-promoted alkyne azide cycloaddition for the functionalization of poly(amide)-based dendrons and dendrimers. *J Am Chem Soc* 132(11):3923–3931.
9. Ornelas C, Pennell R, Liebes LF, Weck M (2011) Construction of a well-defined multifunctional dendrimer for theranostics. *Org Lett* 13(5):976–979.
10. Kim C, et al. (2001) Supramolecular assembly of amide dendrons. *J Am Chem Soc* 123(23):5586–5587.
11. Rannard S, Davis N, McFarland H (2000) Synthesis of dendritic polyamides using novel selective chemistry. *Polym Int* 49(9):1002–1006.
12. Ruiz-Sanchez AJ, et al. (2015) Synthesis of all-aliphatic polyamide dendrimers based on a 3,3′-diaminopivalic acid scaffold. *Polym Chem* 6(16):3031–3038.
13. Mesa-Antunez P, et al. (2016) Fluorescent BAPAD dendrimeric antigens are efficiently internalized by human dendritic cells. *Polymers (Basel)* 8(4):111.
14. Newkome RG, Shreiner DC (2007) Poly(amidoamine), polypropylenimine, and related dendrimers and dendrons possessing different 1 → 2 branching motifs: An overview of the divergent procedures. *Polymer (Guildf)* 49(1):1–173.
15. Denkewalter RG, Kolc JF, Lukasavage WJ (1983) Macromolecular highly branched homogeneous compound. US Patent 4,410,688.
16. Rosen BM, et al. (2009) Dendron-mediated self-assembly, disassembly, and self-organization of complex systems. *Chem Rev* 109(11):6275–6540.
17. Hawker CJ, Fréchet JMJ (1990) Preparation of polymers with controlled molecular architecture. A new convergent approach to dendritic macromolecules. *J Am Chem Soc* 112(21):7638–7647.
18. Wooley KL, Hawker CJ, Fréchet JMJ (1991) Hyperbranched macromolecules via a novel double-stage convergent growth approach. *J Am Chem Soc* 113(11):4252–4261.
19. Naylor AM, Goddard WA, III, Kiefer GE, Tomalia DA (1989) Starburst dendrimers. 5. Molecular shape control. *J Am Chem Soc* 111(6):2339–2341.
20. Percec V, Cho W-D, Mosier PE, Ungar G, Yeardley DJP (1998) Structural analysis of cylindrical and spherical supramolecular dendrimers quantifies the concept of monodendron shape control by generation number. *J Am Chem Soc* 120(43):11061–11070.
21. Maiti PK, Cagin T, Wang G, Goddard WA, III (2004) Structure of PAMAM dendrimers: Generations 1 through 11. *Macromolecules* 37(16):6236–6254.
22. Percec V, et al. (2000) Design and structural analysis of the first spherical monodendron self-organizable in a cubic lattice. *J Am Chem Soc* 122(17):4249–4250.
23. Rosen BM, et al. (2009) Predicting the structure of supramolecular dendrimers via the analysis of libraries of AB_3 and constitutional isomeric AB_2 biphenylpropyl ether self-assembling dendrons. *J Am Chem Soc* 131(47):17500–17521.
24. Percec V, et al. (2006) Synthesis and retrostructural analysis of libraries of AB_3 and constitutional isomeric AB_2 phenylpropyl ether-based supramolecular dendrimers. *J Am Chem Soc* 128(10):3324–3334.
25. Percec V, Cho W-D, Ungar G, Yeardley DJP (2001) Synthesis and structural analysis of two constitutional isomeric libraries of AB_2-based monodendrons and supramolecular dendrimers. *J Am Chem Soc* 123(7):1302–1315.
26. Esfand R, Tomalia DA (2001) Poly(amidoamine) (PAMAM) dendrimers: From biomimicry to drug delivery and biomedical applications. *Drug Discov Today* 6(8): 427–436.
27. Duncan R, Izzo L (2005) Dendrimer biocompatibility and toxicity. *Adv Drug Deliv Rev* 57(15):2215–2237.
28. Lee CC, MacKay JA, Fréchet JMJ, Szoka FC (2005) Designing dendrimers for biological applications. *Nat Biotechnol* 23(12):1517–1526.
29. Kannan RM, Nance E, Kannan S, Tomalia DA (2014) Emerging concepts in dendrimer-based nanomedicine: From design principles to clinical applications. *J Intern Med* 276(6):579–617.
30. Svenson S, Tomalia DA (2005) Dendrimers in biomedical applications—reflections on the field. *Adv Drug Deliv Rev* 57(15):2106–2129.
31. Svenson S (2015) The dendrimer paradox—high medical expectations but poor clinical translation. *Chem Soc Rev* 44(12):4131–4144.
32. De Gennes PG, Hervet H (1983) Statistics of "Starburst" polymers. *J Phys Lett* 44(9): L-351–L-360.
33. Lescanec RL, Muthukumar M (1990) Configurational characteristics and scaling behavior of starburst molecules: A computational study. *Macromolecules* 23(8): 2280–2288.
34. Mourey TH, et al. (1992) Unique behavior of dendritic macromolecules: Intrinsic viscosity of polyether dendrimers. *Macromolecules* 25(9):2401–2406.
35. Ihre H, Hult A, Söderlind E (1996) Synthesis, characterization, and ^{1}H NMR self-diffusion studies of dendritic aliphatic polyesters based on 2,2-bis(hydroxymethyl)propionic acid and 1,1,1-tris(hydroxyphenyl)ethane. *J Am Chem Soc* 118(27):6388–6395.
36. Ihre H, Padilla De Jesús OL, Fréchet JMJ (2001) Fast and convenient divergent synthesis of aliphatic ester dendrimers by anhydride coupling. *J Am Chem Soc* 123(25): 5908–5917.
37. García-Gallego S, Nyström AM, Malkoch M (2015) Chemistry of multifunctional polymers based on bis-MPA and their cutting-edge applications. *Prog Polym Sci* 48: 85–110.
38. Percec V, et al. (2010) Self-assembly of Janus dendrimers into uniform dendrimersomes and other complex architectures. *Science* 328(5981):1009–1014.
39. Peterca M, Percec V, Leowanawat P, Bertin A (2011) Predicting the size and properties of dendrimersomes from the lamellar structure of their amphiphilic Janus dendrimers. *J Am Chem Soc* 133(50):20507–20520.
40. König W, Geiger R (1970) [A new method for synthesis of peptides: Activation of the carboxyl group with dicyclohexylcarbodiimide using 1-hydroxybenzotriazoles as additives]. *Chem Ber* 103(3):788–798. German.
41. Batz H-G, Franzmann G, Ringsdorf H (1972) Model reactions for synthesis of pharmacologically active polymers by way of monomeric and polymeric reactive esters. *Angew Chem Int Ed Engl* 11(12):1103–1104.
42. El-Faham A, Albericio F (2011) Peptide coupling reagents, more than a letter soup. *Chem Rev* 111(11):6557–6602.
43. Jhon MS, Cho U-L, Kier LB, Eyring H (1972) Molecular orbital studies of ethylenediamine conformations. *Proc Natl Acad Sci USA* 69(1):121–123.
44. Boiocchi M, et al. (2004) The influence of the boat-to-chair conversion on the demetallation of the nickel(II) complex of an open-chain tetramine containing a piperazine fragment. *Dalton Trans* 2004(4):653–658.
45. Paital AR, et al. (2009) Structure and dimensionality of coordination complexes correlated to piperazine conformation: From discrete $[Cu^{II}_2]$ and $[Cu^{II}_4]$ complexes to a $\mu_{1,3}$-N_3^- bridged $[Cu^{II}_2]_n$ chain. *Dalton Trans* 2009(8):1352–1362.
46. Tomalia DA, Khanna SN (2016) A systematic framework and nanoperiodic concept for unifying nanoscience: Hard/soft nanoelements, superatoms, meta-atoms, new emerging properties, periodic property patterns, and predictive Mendeleev-like nanoperiodic tables. *Chem Rev* 116(4):2705–2774.
47. Zasloff M (2002) Antimicrobial peptides of multicellular organisms. *Nature* 415(6870): 389–395.
48. Fernandez-Lopez S, et al. (2001) Antibacterial agents based on the cyclic D,L-α-peptide architecture. *Nature* 412(6845):452–455.
49. Porter EA, Wang X, Lee HS, Weisblum B, Gellman SH (2000) Non-haemolytic β-amino-acid oligomers. *Nature* 404(6778):565.
50. Hamuro Y, Schneider JP, DeGrado WF (1999) De novo design of antibacterial β-peptides. *J Am Chem Soc* 121(51):12200–12201.
51. Tew GN, et al. (2002) De novo design of biomimetic antimicrobial polymers. *Proc Natl Acad Sci USA* 99(8):5110–5114.
52. Kuroda K, DeGrado WF (2005) Amphiphilic polymethacrylate derivatives as antimicrobial agents. *J Am Chem Soc* 127(12):4128–4129.
53. Chongsiriwatana NP, et al. (2008) Peptoids that mimic the structure, function, and mechanism of helical antimicrobial peptides. *Proc Natl Acad Sci USA* 105(8): 2794–2799.
54. Fields RD, Lancaster MV (1993) Dual-attribute continuous monitoring of cell proliferation/cytotoxicity. *Am Biotechnol Lab* 11(4):48–50.
55. Ebeling W, et al. (1974) Proteinase K from *Tritirachium album* Limber. *Eur J Biochem* 47(1):91–97.
56. Wang J, Wolf RM, Caldwell JW, Kollman PA, Case DA (2004) Development and testing of a general amber force field. *J Comput Chem* 25(9):1157–1174.
57. Carvalho ATP, Fernandes PA, Ramos MJ (2007) Parameterization of AZT—a widely used nucleoside inhibitor of HIV-1 reverse transcriptase. *Int J Quantum Chem* 107(2): 292–298.
58. Phillips JC, et al. (2005) Scalable molecular dynamics with NAMD. *J Comput Chem* 26(16):1781–1802.
59. Humphrey W, Dalke A, Schulten K (1996) VMD: Visual molecular dynamics. *J Mol Graph* 14(1):33–38, 27–28.
60. Michaud-Agrawal N, Denning EJ, Woolf TB, Beckstein O (2011) MDAnalysis: A toolkit for the analysis of molecular dynamics simulations. *J Comput Chem* 32(10):2319–2327.
61. Sarker SD, Nahar L, Kumarasamy Y (2007) Microtitre plate-based antibacterial assay incorporating resazurin as an indicator of cell growth, and its application in the in vitro antibacterial screening of phytochemicals. *Methods* 42(4):321–324.